Combined Effects of Surface Oxidation and Interfacial Intermetallic Compound Growth on Solderability Degradation of Electrodeposited Tin Thin Films on Copper Substrate due to Isothermal Ageing

Jing Wang,[a] Guang Chen,[a] Fulong Sun,[a,b,c] Zhaoxia Zhou,[d] Zhi-Quan Liu,[b,c] Changqing Liu,[a*]

a – Wolfson School of Mechanical, Electrical and Manufacturing Engineering, Loughborough University, Loughborough, LE11 3TU, United Kingdom

b – Institute of Metal Research, Chinese Academy of Sciences, Shenyang 110016, China

c – University of Chinese Academy of Sciences, Beijing 100049, China

d – Loughborough Materials Characterisation Centre, Department of Materials, Loughborough University, Loughborough, LE11 3TU, United Kingdom

* Corresponding author – Email: C.Liu@lboro.ac.uk

Abstract

We report new insights into the solder wettability degradation of Sn thin films on Cu under 155°C isothermal ageing. A multiscale wettability degradation model was established, reflecting quantitatively the surface oxidation and interfacial intermetallic compound (IMC) growth, on the basis of solder wetting behaviour. The thermal oxidation of Sn exhibited heterogeneous inward thickening, lateral expanding and outward platelet-like growth, forming nanocrystalline, oxygen-deficient SnO_2 with pronounced voiding/cracking propensity. Unlike a commonly held belief that the initial wettability loss is due to surface-exposing and oxidation of IMCs, it was found from dual combined effects of inward surface oxidation and outward IMC growth.

Keywords: A. Electronic materials; A. Intermetallics; A. Metal coatings; A. Tin; B. STEM; C. Oxidation.

1. Introduction

The solder wettability degradation of electronics components during storage poses a serious issue in the challenge of defect-free soldering. This is especially true in an era of lead-free technology, where the prevailing Sn-Ag-Cu (SAC) ternary alloy solders exhibit

inferior wetting abilities and entail narrower process windows, compared to that of conventional Sn-Pb solders [1, 2]. The natural solderability degradation of Sn-based metal finishes on Cu substrate has been attributed to both surface Sn oxidation and interfacial Sn-Cu IMC growth, with the former dominant in early stages whilst the latter claimed to govern the eventual wettability loss [3]. Various preconditioning approaches have been exploited to accelerate the solderability degradation as such to help emulate long-term degradation profiles within reasonably short periods of time. These preconditions [4, 5] include dry bake (i.e. isothermal ageing in air at 150 or 155°C), steam conditioning (i.e. isothermal ageing in steam at 93 or 100°C) and damp heat (i.e. exposure to 72°C combined with RH 85%). Recent years have seen increasing importance given to the dry bake approach due to high result repeatability and consistency. However, only a few published works have taken a systematic analysis of the solderability degradation and preconditioning of Sn-based finishes [3, 6]. The age-old question concerning the eventual solder wettability loss of the Sn coated Cu systems has remained largely unresolved. The present study aims at understanding the microstructural evolution characteristics of Sn thin films on Cu under the dry bake method from contemporary materials science viewpoints, and attempts to elucidate the precise origins for the solder wettability loss.

Diverging opinions existed concerning whether the interfacial Cu-Sn IMCs tends to promote solder spreading. One perspective [7-10] holds that the surfaces of Cu_6Sn_5-based IMCs exhibit reasonably good solderability towards Sn-based solders, as compared with that of, e.g. a Cu surface. Such a lyophilicity has been correlated, primarily to an increased wetting driving force provided by the energy liberation of interfacial reactions between molten Sn and solid Cu-Sn IMCs [7, 10, 11], and secondarily, to enhanced capillary action induced by surface roughness of the complex-shaped IMCs [7, 8]. On the other hand, there have been evidences suggesting that, once exposed to air, the Cu-Sn IMC surface tends to form oxides, practically rendering the flux ineffective and prohibiting solder wetting [3, 12]. It is for this reasoning that the exposing of the IMCs to Sn film surface has been technically deemed as an indicator for the eventual solderability loss. Nonetheless, neither of the hypotheses considers the concurrent oxidation of Sn metal

surface, which presents a competing mechanism to the interfacial IMC growth and becomes even more nontrivial when thermal ageing is applied accelerating both the processes. The thermal oxidation of Sn has been the subject of numerous investigations [13-18]. The oxidation kinetics and oxide compositions have been said to show dependence on temperature [13-14]. Notably, a transition in the oxidation process occurs between 130 and 180°C [15], where the precondition temperature used in this study (i.e. 155°C) falls in. Below this temperature range, amorphous Sn oxides tend to form, following direct logarithmic rate laws potentially controlled by, e.g. phase boundary reaction and diffusion. Above the stated range, the oxides formed generally become crystalline, obeying parabolic growth kinetics controlled by diffusion [13]. The nature of the oxidation products has nevertheless remained equivocal [3, 13, 16, 18]. The ambiguity largely stems from difficulties in discriminating between stannous (SnO) and stannic (SnO_2) oxide in ultra-thin film formats [19], and also inherently from possible spontaneous conversion of SnO into SnO_2 in air [20, 21]. The structural defects within the thermally grown Sn oxides, e.g. through-thickness cracking and interior voiding, are limitedly understood. Also, it remains to be answered in terms of how the Sn oxide formation contributes to the local interfacial chemistry and structure over the course of solder spreading. The present work aims to address these questions with microstructural descriptions.

Wetting balance analysis was adopted as per J-STD 002D [4] to assess solder wettability, which induces an upward, meniscus rise of liquid solder upon vertically positioned specimen surface. The method decouples gravitational force from the wetting driving force and is useful for observations of poor wetting interactions. The solder meniscus rise may involve partial dissolution of the specimen surface (i.e. dissolutive wetting) and/or formation of intermetallic phases (i.e. chemical reactive wetting). The wetting process is hence likely to be driven by capillary forces and interfacial dissolution/reactions, and resisted by surface pinning mechanisms (e.g. oxides), liquid solder viscosity and gravitational force [7]. The temporal and spatial evolution of the wetting process may be further complicated when the sample surface exhibited roughness and chemical

inhomogeneity [7]. All these effects may contribute collectively to the final triple line configuration and wetting kinetics [22], which could far deviate from the Young equilibrium based on a simple inert wetting model [23]. In terms of dissolutive wetting, fusible materials such as Sn metal dissolve upon solder spreading, which results in a macroscopically non-planar solid IMC/liquid interface [23]. For chemical reactive wetting, interfacial reactions have been reported to occur between liquid Sn-based solder and Cu-Sn IMCs, resulting in further morphological evolution of the IMCs [7, 10, 11]. For both the wetting models, the final triple line configuration has been suggested to directly correlate to the final three-dimensional interfacial chemistry and structures (i.e. based on interfacial energy terms, $\Delta\sigma_r$) [24, 25], rather than to the intensity of the interfacial reactions (i.e. based on Gibbs free energy terms, ΔG_r) [22]. The present paper concerns mainly with physicochemical mechanisms which account for the solder wettability degradation of Sn layers on Cu upon isothermal ageing, with a treatment of the variations in various triple line wetting driving forces.

2. Experimental

2.1. Materials

2.5 μm thick, pure Sn electrodeposited specimens employed in this study were electroplated under galvanostatic conditions using a proprietary process by Huawei Technologies Ltd. (Shenzhen, China), on both sides of Cu sheet substrates following a configuration (20 mm × 5 mm × 0.2 mm).

2.2. Preconditioning and Characterisations

Dry bake was conducted at 155°C with bare samples positioned in an ageing oven in air. No specific pretreatment or post-treatment was conducted for the dry bake precondition. Wettability test was performed using a Robotic Process Systems Six-Sigma wetting balance tester. After calibration, the wetting balance tests utilised an optimised condition, with solder bath of SAC305 alloy maintaining at 245°C, a ROL0 flux (Alpha rosin flux 800), immersion depth of 7 mm, immersion/emersion speed of 25 mm/s, a dwell time of 5 s and no pre-heat. At least 10 samples were assessed for each condition.

The surface morphology of thermally aged Sn metal thin films was analysed utilising a FEGSEM (JOEL 7800F) at low accelerating voltage (2 kV) to enable surface-specific imaging of oxide formation. The oxide thickness was measured through XPS compositional depth profiling using a Thermo Scientific K-Alpha X-ray Photoelectron Spectrometer with an Al source, in conjunction with argon ion monomer sputtering. To analyse the microstructural, compositional and crystallographic characteristics of surface oxides, conventional and high resolution TEM (C-/HR-TEM) were conducted using a FEI Tecnai F20 operating at 200 kV. The EDX elemental maps were collected in the scanning TEM mode, in single frame using long dwell time to minimise beam spread and drift during data acquisition. The TEM specimens were prepared on molybdenum grids using a standard lift-out method on a FEI Nova SEM/FIB dual-beam microscope, fitted with a liquid gallium ion source and operating at 30 kV accelerating voltage. Electron-beam and ion-beam platinum were applied on site to protect the TEM samples from ion milling damage. The thickness of the interfacial IMCs was measured from the cross-sectional view prepared from FIB milling [26], based on multiple sample locations for data representativeness. After 5 s solder immersion of wetting balance test, the meniscus rise front was analysed from both surface and cross-sectional views.

3.0 Results

3.1 Effect of thermal preconditioning on surface oxidation

The representative surface morphology of 2.5 μm thick pure Sn films on Cu as a function of isothermal ageing time up to 32 hr is presented in Fig. 1. Prior to any thermal ageing (Fig. 1a), the Sn film surface was smooth without any appreciably sized features. As the ageing time increased to 4 hr, the film surface saw discrete distribution of micron-sized, patch-like features. The O content was generally elevated on these features from EDX analysis, signifying the heterogeneous thickening of Sn oxides. This is corroborated with STEM results presented in the next. The patch-like features manifested themselves in darker contrast compared to that of the surrounding region, from secondary electron imaging at a relatively low accelerating voltage at 2 kV. From 4 hr, through 8 hr and further to 12 hr, the distribution density of the features became increased. At 12 hr (Fig.

1d), spike- and spine-like features were observed to grow outward from the preferential oxide growth centers (‘patches’), developing into platelets. At 16 hr (Fig. 1e), the preferential oxide growth centers had spread laterally, impinging on each other and eventually giving rise to complete surface coverage. The surface morphology remained largely unchanged when the ageing time was doubled to 32 hr (Fig. 1f). This was accompanied by cracking on the Sn oxide surface, indicating the build-up of compressive stress arising from the specific volume difference (~ 20 %) between Sn metal and oxides [13].

The thickness of thermally promoted oxides on the Sn thin film surface was assessed using XPS compositional profiling measurements, over relatively large sampling areas (400 μm × 400 μm) in attempts to average out compositional and oxide thickness variations. As a simplified treatment, the oxide thickness was determined at which the relative percentage of O is equal to half of its maximum value. Plotted in semi-logarithmic scale in Fig. 2, after an initial period of steady oxidation rate up to below 8 hr, the Sn oxidation kinetics started to slow down, merging into a direct logarithmic relationship up to 32 hr. This relationship can be expressed in the form of,

$$L = 25.7 \ln (t + 83.7) - 146.7 \quad (1)$$

Where L denotes the XPS-derived Sn oxide film thickness reacted at time t. Such logarithmic kinetics characteristics were largely in agreement with several published works using vacuum microbalance measurements [13, 27]. Beyond 8 hr as the oxidation kinetics started to decelerate, the measured data became increasingly fluctuating between analyses (i.e. reflected in increased standard deviations), which was presumably due to oxide cracking permitting direct ingress of gaseous oxygen to underlying Sn metal perturbing oxidation kinetics.

Figures 3-4 show STEM bright field images and the EDX maps of selected areas from the cross-sections of the isothermally aged samples, whilst Figures 5-6 present TEM/HRTEM images providing spatially resolved, microstructural and crystallographic

information of the surface oxides. At 12 hr, a TEM cross-sectional specimen was prepared to incorporate both the platelet-grown oxide patch features (in Fig. 1d) and adjacent region for ready comparisons, as shown in Fig. 3. The patch-like oxide regions exhibited more rapid milling rates compared to that of Sn and Pt, and had seen only small portions remnant (See examples in Fig. 5 c-e) from the FIB final thinning. But still, the patch outline was evidently defined by the overlying e-beam deposited Pt and underlying Sn metal, giving a shallow pit-like geometry with an in-plane width of ca. 1600 nm and depth of ca. 100 nm. Another oxide patch with a much smaller width of ca. 250 nm was also observed, which points to the possibility of an oxide patch at its early growth (i.e. embryo) stage. Apart from the two patches, the remaining surface oxide appeared to be relatively thin. Also, preferential oxide thickening where Sn grain boundaries intersect with oxide/metal interface was evident, suggesting the role of grain boundary as straightforward pathways for reactant transport [28]. From EDX mapping (Fig. 3b), the oxides were generally enriched with Sn and O, without any concurrent elevation of Cu content, suggesting the sole presence of Sn oxides. From HRTEM observations, all the oxides, including patch-free (Fig. 5a), embryo patch (Fig. 5b) and developed patch regions (Fig. 5c-e), showed distribution of equiaxed nanocrystals with a typical in-plane size of ca. 5 nm, taking in a crystal structure of tetragonal SnO_2 and with most densely packed, low index planes of (110) (d-spacing = 0.335 nm) and (101) (d-spacing = 0.264 nm) observed (analysed as per PDF 41-1445). The patch-free region (Fig. 5a) demonstrated a ca. 6 nm thick oxide layer, but in its vicinity within the Sn metal, SnO_2 nanocrystals with in-plane sizes exceeding 10 nm were observed as well, indicative of a superficial zone beneath the metal/oxide interface consisting of a conglomerate of SnO_2 and Sn metal crystals. In the embryo patch region (Fig. 5b), the metal/oxide phase boundary was not clearly defined. A number of randomly oriented SnO_2 nanocrystal clusters with lighter contrast were observed, signifying the presence of nano-sized cavities. In the developed patch region, oxide voiding became evident (Fig. 5c). Fig. 5d gives an example of nodular oxide formation close to the metal/oxide phase boundary, whilst Fig. 5e is believed to present a FIB-thinning remnant of a platelet structure grown on the patch surface. In both cases, it was recognised that these oxide formations

developed outward from a thin oxide layer (of a few nm), instead of directly growing from bare metal surface. For the oxide platelet structure (Fig. 5e), the nanograins were preferentially distributed along the out-of-plane direction. The EDX-measured compositions of the oxides were generally close to non-stoichiometric Sn_2O, with a gradual reduction in the relative atomic percentage of O as the distance to the oxide surface increases. This oxygen deficiency is a characteristic of non-ideal, n-type oxides like SnO_2, signifying a high degree of ionic lattice defects, e.g. in the form of ionised oxygen vacancies ($V_{\dot{O}}$) [19, 28]. At 16 hr (Fig. 4), the entire Sn surface (Fig. 1e) had seen coverage of the patch-like oxide structure, albeit delaminated at certain locations. Oxide cavities were found across the surface and typically close to the metal/oxide interface, as demonstrated in Fig. 6a. This can be attributed to the migration, precipitation and clustering of oxygen vacancies. The oxides were again observed to be tetragonal SnO_2 (Fig. 6b) at a rough composition of Sn_2O, even at locations where the Cu-Sn IMC growth had penetrated to the Sn coating surface (Fig. 6c).

3.2 Effect of thermal preconditioning on interfacial IMC growth

The effect of isothermal ageing at 155°C on the interfacial Cu-Sn IMC growth has been investigated through FIB-SEM observations, from which the thickness variations of the IMCs and unreacted Sn metal are plotted in Fig. 7. It was found that the Cu-Sn IMC thickness largely obeyd the classic parabolic kinetics relationship within the range from 4 hr to16 hr. Beyond 16 hr when the IMCs started to locally penetrate to the Sn metal/oxide interface (as demonstrated in Fig. 4), the IMC thickness increment entered stagnation, departing from a simple, diffusion controlled law and up to when the entire Sn coating had been converted into Cu-Sn IMCs by 32 hr. The deceleration can be ascribed to reduced avaliablity of Sn metal and/or to competing mechanisms such as Sn oxidation.

3.3 Effect of thermal preconditioning on wetting balance analyses

Figure 8a shows representative wetting force-time curves of 2.5 μm thick Sn thin films

after having subject to varied periods of dry bake condition at 155°C. Two subtracted solderability indices, zero cross time (ZCT) and maximum wetting force (F_{max}), were presented in Fig. 8b, which provides gauging of both the rate and degree of solder meniscus rise upon specimen surfaces, respectively. ZCT refers to the measured wetting force returning to zero, whilst F_{max} denotes the maximum wetting force achieved on the time-force curve. With prolonging thermal ageing from 0 hr to 32 hr, there had been a steadily increasing suppression upon the meniscus rise, reflected in extending ZCT and declining F_{max} until a failure of positive wicking had occurred at 16 hr where a reading of ZCT became not possible. For all the conditions investigated, the wetting process arrived at equilibrium within 2.5 s.

Figures 9-10 present a surface view of the resolidified meniscus rise front of the thermally aged Sn on Cu samples after wetting balance tests, with corresponding EDX maps. At 12 hr (Fig. 9) when the solderability was deemed lost from wetting balance test, it is interesting to note that meniscus rise did occur, albeit very limitedly. A curved solder spreading boundary was identified on the sample surface, which was preceded by a compact unsoldered area and followed by detached and fractured Sn oxide crusts on the resolidified SAC305 solder surface. EDX mapping (Figs. 9b-f) suggested that the solder liquid migrated beneath Sn oxides, with the latter peeled off from volume expansion by solder ingress. The volume expansion is evidenced from the absence of underlying Cu-Sn IMCs on the EDX maps, indicaitive of a thickening of the overlying fused Sn layer. A Sn oxide region immediately ahead of the solder spreading front (as outlined in Fig. 9b) demonstrated such a thickening of intermediate Sn layer, which imlies an initial stage of the oxide detaching. Also there was a Ag depletion zone immediately behind the solder spreading front, with a number of Ag-enriched channels linked between spreading front and the bulk of the solder. At 16 hr (Fig. 10), albeit macroscopically failing the wetting balance test, the meniscus rise front exhibited similar microstructural characteristics to 12 hr, suggesting little difference in the solder wetting mechanism between 12 hr and 16 hr.

As indicated in Fig 10b, a TEM cross-sectional specimen was lifted out from the solder

spreading front of the Sn-coated Cu sample thermally aged for 16 hr after the wetting balance test. The STEM bright field image and the corresponding EDX maps of the specimen is presented in Fig. 11. It became evident that the previous columnar grained Sn zone intermediate between surface oxide and interfacial Cu-Sn IMCs had fused with the molten SAC305 solder through imbibition under wetting conditions, forming a thickened Sn-enriched zone with coarsened Sn grains (grain size was presumably larger than the TEM sampling area). There was a submicron Cu-Sn IMC particle spalled from the bulk of the IMC structures, suggesting possible evolution of the IMCs during up to 5 s of solder spreading. It is interesting to note that Ag was observed to segregate to beneath the surface oxide and to the close vicinity of the surfaces of scallop-shaped Cu-Sn IMCs, as nano-sized, Ag-rich precipitates. These suggest Ag atoms were highly diffusive and tensioactive, which contributed to the in-situ modification of the interfaces between liquid solder and solid IMC structure.

4. Discussions

To understand the roles of surface oxidation and interfacial Cu-Sn IMC growth in the solder wettability degradation profile, we attempt to identify temporal and spatial correlation between their microstructural evolution characteristics, wetting forces and the solder advancing front's features resulted from wetting test. A failure of meniscus rise had notably emerged with an increase in the isothermal ageing time from 12 hr to 16 hr. Direct comparisons between these two intervals are hence pivotal in elucidating the specific origins accounting for the solder wettability loss.

4.1 Surface Oxidation as a Wetting Barrier

Here we depict the microstructural evolution of the surface oxides in Fig. 12. After having uniformly grown into a thickness of ca. 5 nm (Fig. 12a), the heterogeneous thickening of Sn oxides initiated from certain Sn grain boundaries intersecting with the surface, through the formation of nanocrystalline SnO_2 grains with a mean size of ca. 5 nm. These result in the formation of discrete oxide patch embryos with unsmooth oxide/metal interface, together with the onset of nano-sized oxide cavity (Fig. 12b). With increasing ageing time,

the ‘oxide patches’ saw a steady increase in distribution density, together with lateral spreading and further outward growth into platelet- and spine-shaped formations (Fig. 12c). This is extensively accompanied by the nucleation and coarsening of oxide cavities as well as cracking, presenting potential weaknesses in the oxide microstructural integrity permitting liquid solder ingress into the metal/oxide interface. The evolution of the nano-sized cavities into micron-sized, isolated voids imply a history of Ostwald ripening through the Kirkendall effect [30], where oxygen vacancies diffuse and supersaturate around existing void surfaces, subsequently into precipitation and further coalescence [31]. From 12 hr to 16 hr, the Sn thin film surface had attained full coverage of the rough ‘oxide patch’ morphology. From the perspective of solder wetting, the complete coverage of oxide patching at 16 hr is believed to provide increased wetting barrier efficacy compared with that of the heterogeneously thickened oxide at 12 hr. First, it appeared that the solder spreading generally propagates *through* the surface cracked oxide and *beneath* the surface oxide by fusing the Sn metal. This suggests limited lyophilicity and solubility of the surface oxides towards liquid SAC305 solder. A general elevation of the oxide thickness will increase difficulties for solder penetration through the oxide and also for peeling off the oxide layer. Second, beyond 16 hr the exposed IMC structures are thought to act as point obstacles against progressive dissolutive wetting of fusible Sn metal and against fusion-assisted oxide peeling. Therefore, with increasing ageing time, the surface oxides play an ever increasingly decisive role in diminishing the wetting driving force, despite the universal presence of cracking and voiding may provide straightforward access for liquid solder ingress.

4.2 Exposing of Cu-Sn IMCs as a Wetting Barrier

As presented in Fig. 7, the average consumption rate of the Sn metal layer resulted from interfacial Cu-Sn IMC growth largely conformed to a diffusion controlled, parabolic rate law, before entering stagnation. From 12 hr to 16 hr, the thickness of unreacted Sn layer showed a slight reduction from 0.42 μm to 0.31 μm. At 16 hr the metal/oxide interface had only seen very *limited* penetration of IMCs, the oxides formed on which demonstrated composition and crystal structure similar to that of Sn metal. Therefore, simply attributing

the wettability loss at 16 hr to the oxidation of the exposed IMC surfaces is hardly valid. Combining the characteristics of surface oxidation and interfacial IMC growth, the microstructural evolution of solder spreading front for the thermally aged, Sn coated samples is expressed in Fig. 13. Liquid solder can hardly wet the oxide surface owing to the low surface energy of the latter. Rather, the flux-guided solder tends to attack 'weak spots' in the oxide structure, e.g. a thin oxide region or through-thickness crack/void, and subsequently to fuse the Sn metal through a semi-closed capillary-driven infiltration mechanism [32]. Given the observations of the IMCs spalled into the liquid solder (Fig. 11), the solder wetting event over the course of up to 5 s did induce interfacial reactions between the liquid solder and Cu-Sn IMCs, and hence shall contribute an interfacial energy supply to the wetting driving force. Such interfacial reactions involved double in-situ modifications [24] of the interface: adsorption of Ag_3Sn IMC nanoparticles at the liquid side [33] and formation of Cu-Sn-based IMCs at the solid side. However, upon progressive IMC growth, such a wetting driving force is likely to be outweighed by the limited availability of Sn metal for dissolutive wetting. This, together with a complete coverage of oxide 'patches', is believed to induce the eventual solder wettability loss.

4.3 Degradation of Wetting Force

Under the inert wetting conditions, the instantaneous wetting driving force, $F_i(t)$, is expressed as,

$$F_i(t) = \sigma_{SV}^0 - \sigma_{SL}^0 - \sigma_{LV}^0 \cos\theta(t) \quad (2)$$

Where σ_{SV}^0, σ_{SL}^0 and σ_{LV}^0 refer to static interfacial energy between solid and vapor, solid and liquid, liquid and vapor, respectively, $\theta(t)$ is the instantaneous contact angle. For the present system where dissolutive wetting of Sn, interfacial reaction at the solder/IMC interface and surface oxide as a wetting barrier need to be considered, the instantaneous wetting driving force per unit length, $F_r(t)$, is expressed as,

$$F_r(t) = \sigma^0_{S(Sn)V}(t) - (\sigma^0_{S(Sn)L(SAC305)} + \Delta\sigma_{Sn}(t) + \Delta\sigma_{IMC}(t)) -$$

$$(\sigma^0_{L(SAC305)V}\cos\theta(t) + \Delta\sigma_{Oxide}(t)) \quad (3)$$

Where $\sigma^0_{S(Sn)V}(t)$ denotes the instantaneous interfacial energy between Sn metal and air encountered beneath the oxide (e.g. rendered available through oxide cracking or voiding), $\sigma^0_{S(Sn)L(SAC305)}$ refers to the interfacial energy between solid Sn metal and liquid SAC305 solder, $\Delta\sigma_{Sn}(t)$ refers to the instantaneous interfacial energy liberated from dissolutive wetting of Sn per unit area, $\Delta\sigma_{IMC}(t)$ refers to the instantaneous interfacial energy per unit area released from the formation of IMCs at the interface between liquid solder and existing Cu-Sn IMCs, $\sigma^0_{L(SAC305)V}$ refers to the instantaneous interfacial energy per unit area between liquid SAC305 solder and air. $\Delta\sigma_{Oxide}(t)$ refers to the instantaneous interfacial energy per unit area consumed in the breakage/detachment of oxide at the spreading front. $\theta(t)$ denotes the instantaneous contact angle. It needs to be addressed here that both the apparent liquid-vapor and solid-vapor interfacial energy terms could exhibit sensitivity to time, due to the presence of surface oxide above the solder spreading front governing its contact with the air. It can be inferred from Equation 3 that the dynamic wetting driving force is extremely complex to interpret. The major time-dependent wetting driving forces may include the instantaneous surface tension of Sn metal ($\sigma^0_{S(Sn)V}(t)$), the interfacial energy release from dissolutive wetting of Sn, (-$\Delta\sigma_{Sn}(t)$), and from instantaneous growth of the IMCs (-$\Delta\sigma_{IMC}(t)$), whereas major counteracting forces are thought to consist of the interfacial energy between liquid solder and air ($\sigma^0_{L(SAC305)V}\cos\theta(t)$) and the interfacial energy required to peel off the surface oxide at solder spreading front ($\Delta\sigma_{Oxide}(t)$). With increasing ageing time up to 16 hr, we expect a pronounced diminishing in the driving force from dissolutive wetting of Sn (-$\Delta\sigma_{Sn}(t)$) due to reducing availability of Sn metal, combined with localised IMC penetration to the metal/oxide interface acting as obstacles to pinning the liquid solder propagation. Also there shall be an increasing wetting resisting component from peeling off the surface

oxide ($\Delta\sigma_{Oxide}(t)$) due to progressive oxide thickening. It is hence interesting to note that the role of the interfacial IMC growth in the solder wetting is duplex, i.e. both wetting promoting and inhibiting. The wetting inhibiting effect becomes more dominant as the growing IMCs start to come into proximity with surface oxide layer.

Conclusions

In this work, we have investigated the combined effect of the surface Sn oxidation and interfacial IMC growth on the solder wettability degradation of 2.5 μm thick pure Sn electrodeposits on Cu substrate after 155°C isothermal ageing up to 32 hr. The main findings are summarised as follows,

1) The thermal oxidation of Sn thin films on Cu at 155°C has been systematically characterised. Largely obeying a direct logarithmic rate law, the oxidation exhibited heterogeneous inward thickening at discrete surface locations (formation of 'patches'), accompanied by lateral expanding and outward growth into platelet-like structure. The oxidation products were identified mainly as nanocrystalline tetragonal SnO_2 with high oxygen deficiency and pronounced voiding/cracking propensity.

2) The interfacial Cu-Sn IMC growth largely obeyed diffusion controlled, parabolic kinetics. By 16 hr the metal/oxide boundaries had only seen limited exposing of IMCs. The Sn oxides formed on the exposed Cu_6Sn_5 IMC surface did not demonstrate any significant difference compared to that on Sn metal in terms of crystal structure and composition. These indicate an insignificant role of the IMC surface oxide in the initial solder wettability loss.

3) Based on the wetting balance analysis, the onset of solder wettability loss at 16 hr was found to coincide with a complete coverage of patch-like oxide morphology, together with significant consumption of Sn metal due to interfacial IMC growth.

4) Through microstructural analyses of the solder advancing front from wetting balance

tests, we have found that the surface oxide cracking provided straightforward pathways for penetration of liquid solder; and the penetrated SAC305 solder liquid propagated by fusing with the intermediate Sn metal between surface Sn oxide and underlying Cu-Sn IMCs. A multiscale model incorporating Sn oxidation, intermediate Sn metal consumption and interfacial Cu-Sn IMC growth was proposed to illustrate the solder wettability degradation behaviour. Unlike the commonly held belief that the initial wettability loss is due to the surface-exposing and subsequent oxidation of Cu-Sn IMCs, it was found from low wettability of completely thickened Sn oxide layer, together with reduced availability of fusible Sn metal as a consequence of inward surface oxidation and outward IMC growth.

Acknowledgements

This work was supported by Huawei Technologies, Shenzhen, China [grant number HIPRO20160804]. The authors also acknowledge use of facilities within the Loughborough Materials Characterisation Centre.

Data Availability

The raw/processed data required to reproduce these findings cannot be shared at this time as the data also forms part of an ongoing study.

References

[1] G. C. Wilson, A review of accelerated ageing of printed boards with respect to solderability, Circuit World, 4 (1978) 39-44.

[2] J. M. Song, Y. M. Cheng, C. H. Tsai, Oxidation of liquid solders for die attachment, Corros. Sci., 52 (2010) 4011-4016.

[3] H. L. Reynolds, J. W. Morris, The role of Cu-Sn intermetallics in wettability degradation, J. Electron. Mater., 24 (1995) 1429-1434.

[4] EIA, IPC, JEDEC, Solderability tests for component leads, terminations, lugs, terminals and wires, EIA/IPC/JEDEC J-STD-002D (2013).

[5] IEC, Environmental testing – Part 2-20: Tests – Test T: Test methods for

solderability and resistance to soldering heat of devices with leads, IEC 60068-2 -20 (2008).

[6] T. Hetschel, K. J. Wolter, F. Phillipp, Wettability effects of immersion tin final finishes with lead free solder, Proc. 2nd Electron. Syst. Technol. Conf. (ESTC), (2008) 561-566.

[7] H. Wang, H. Zhao, D. P. Sekulic and Y. Qian, A comparative study of reactive wetting of lead and lead-free solders on Cu and (Cu_6Sn_5/Cu_3Sn)/Cu Substrates, J. Electron. Mater. 37 (2008) 1640-1647.

[8] H. Zhao, H. Q. Wang, D. P. Sekulic and Y. Y. Qian, Spreading kinetics of liquid solders over an intermetallic solid surface. Part 1: eutectic lead solder, J. Electron. Mater. 38 (2009), 1838-1845.

[9] H. Zhao, H. Q. Wang, D. P. Sekulic and Y. Y. Qian, Spreading kinetics of liquid solders over an intermetallic solid surface. Part 2: lead-free solders, J. Electron. Mater. 38 (2009), 1846-1854.

[10] H. Wang, F. Gao, X. Ma, Y. Qian, Reactive wetting of solders on Cu and Cu_6Sn_5/Cu_3Sn/Cu substrates using wetting balance, Scr. Mater. 55 (2006) 823-826.

[11] P. Protsenko, A. Terlain, V. Traskine, N. Eustathopoulos, The role of intermetallics in wetting in metallic systems, Scr. Mater. 45 (2001) 1439-1445.

[12] P. Gordon, T. Hurtony, Investigation of the wetting properties of Cu_6Sn_5 intermetallic compound, Proceedings of 38th International Spring Seminar on Electronics Technology (ISSE), (2015), 315-319.

[13] W. E. Boggs, The oxidation of tin III. The mechanisms of oxidation of pure tin and their dependence on time and oxygen pressure, J. Electrochem. Soc. 108 (1961) 124-129.

[14] W. E. Boggs, R. H. Kachik and G. E. Pellissier, The oxidation of tin I. The kinetics of oxidation of pure tin and the effects of temperature and oxygen pressure, J. Electrochem. Soc. 196 (1961) 6-12.

[15] D. R. Gabe, Mixed oxide films on tin, Surf. Technol. 5 (1977) 463-478.

[16] R. K. Hart, The thermal oxidation of tin, Proc. Phys. Soc. B 65 (1952) 955-956.

[17] R. P. Frankenthal, D. J. Siconolfi, An AES study of the oxidation of a 97Pb-3Sn

alloy, Corros. Sci., 21 (1981), 479-486.
[18] J. M. Song, Y. C. Chang-Chien, B. C. Huang, W. T. Chen, C. R. Shie, C. Y. Hsu, Spectroscopic investigation of oxidized solder surfaces, Corros. Sci., 53 (2011), 2283-2288.
[19] D. A. Asbury and G. B. Hoflund, A surface study of the oxidation of polycrystalline tin, J. Vac. Sci. Technol. A 5 (1987) 1132-1135.
[20] J. T. Abraham, P. V. Thomas, K. G. Gopchandran, B. Joseph, V. K. Vaidyan, Oxidation mechanism involved in thin tin films, Ind. J. Eng. Mater. Sci. 3 (1996) 109-113.
[21] J. Wang, C. Lu, X. Liu, Y. Wang, Z. Zhu, D. Meng, Synthesis of tin oxide (SnO & SnO2) micro/nanostructures with novel distribution characteristic and superior photocatalytic performance, Mater. Des. 115 (2017) 103-111.
[22] F. G. Yost, A. D. Romig, Thermodynamics of wetting by liquid metals. MRS Online Proceedings Library Archive, 108 (1987).
[23] N. Eustathopoulos, M. G. Nicholas, B. Drevet, Wettability at high temperatures, 1st Edition, Pergamon (1999).
[24] N. Eustathopoulos, Mechanisms of wetting in reactive metal/oxide systems, MRS Proceedings 314 (1993) 15-26.
[25] N. Eustathopoulos, Dynamics of wetting in reactive metal/ceramic systems, Acta Mater. 46 (1998) 2319-2327.
[26] J. Wang, G. Chen, H. Forbes, K. Christopoulos, C. Liu, L. Sun, P. Shang, An investigation into the effect of dry bake on the solderability degradation of electrodeposited tin finishes, in Proceedings of 2017 18th International Conferences on Electronic Packaging Technology (ICEPT), 366-271.
[27] S. C. Britton and K. Bright, An examination of oxide films on tin and tinplate, Metallurgia 56 (1957) 163-168.
[28] J. G. Lisoni, L. Goux, T. H. Hoffmann, D. E. Diaz-Droguett, M. Jurczak, Influence of the microstructure on the oxidation of Ni thin films, Corros. Sci. 59 (2012) 282-289.
[29] C. F. Li, Z. Q. Liu, Fabrication of nanocrystalline SnO_2 using electron stimulated oxidation, Nanotechnol. 24 (2013) 205303.

[30] A. D. Smigelskas, E. O. Kirkendall, Zinc Diffusion in Alpha Brass, Trans. AIME 147 (1942) 104.

[31] M. M. Islam, B. Diawara, V. Maurice, P. Marcus, Atomistic modeling of voiding mechanisms at oxide/alloy interfaces, J. Phys. Chem. C 113 (2009), 9978-9981.

[32] W. Liu, D. P. Sekulic, Capillary driven molten metal flow over topographically complex substrates, Langmuir 27 (2011), 6720-6730.

[33] X. Liu, M. Huang, Y. Zhao, C. M. L. Wu, L. Wang, The adsorption of Ag_3Sn nano-particles on Cu-Sn intermetallic compounds of Sn-3Ag-0.5Cu/Cu during soldering, J. Alloys Compd. 492 (2010), 433-438.

Figure Captions

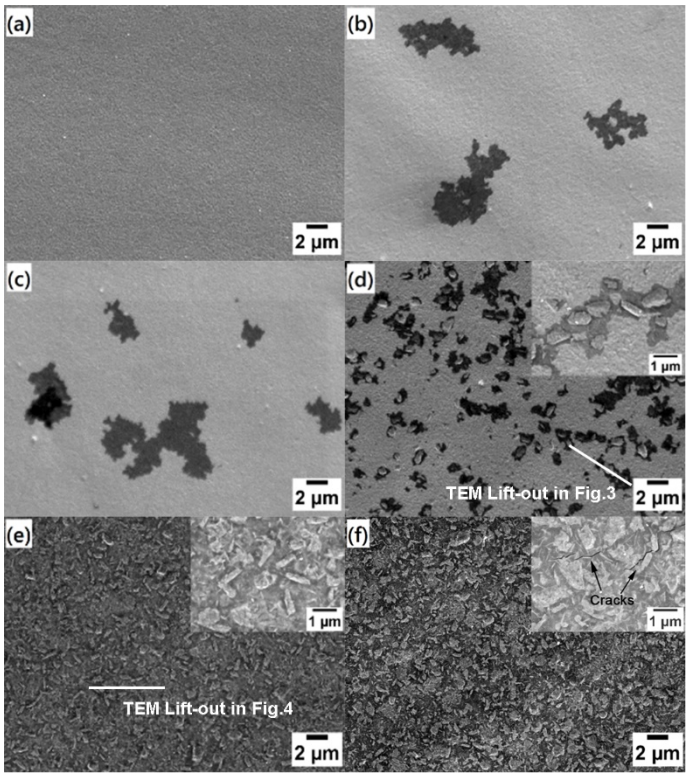

Figure 1 – SEM images illustrating the representative surface morphology of 2.5 µm thick pure Sn finishes on Cu after isothermal ageing at 155°C in air for a) 0 hr, b) 4 hr, c) 8 hr, d) 12 hr, e) 16 hr and f) 32 hr, with selected magnified insets.

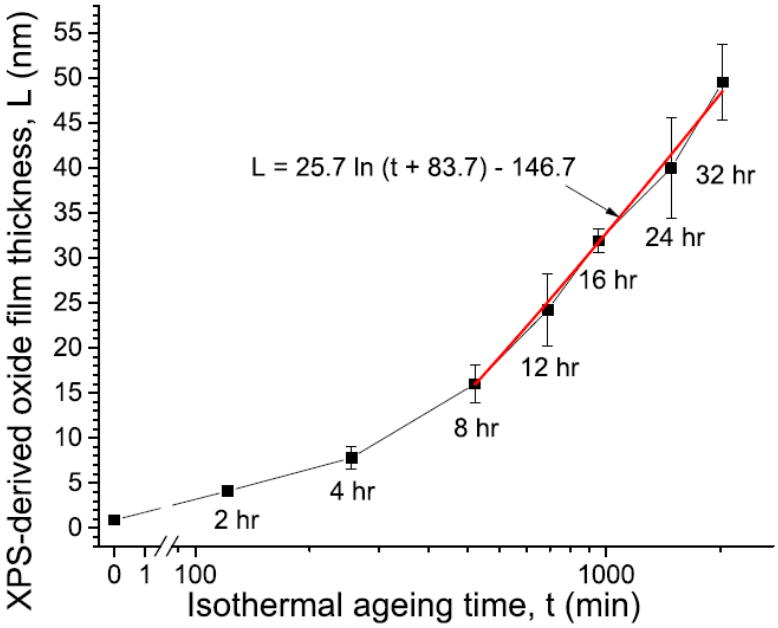

Figure 2 – Log-time plot of XPS-derived Sn oxide film thickness vs. the isothermal ageing time

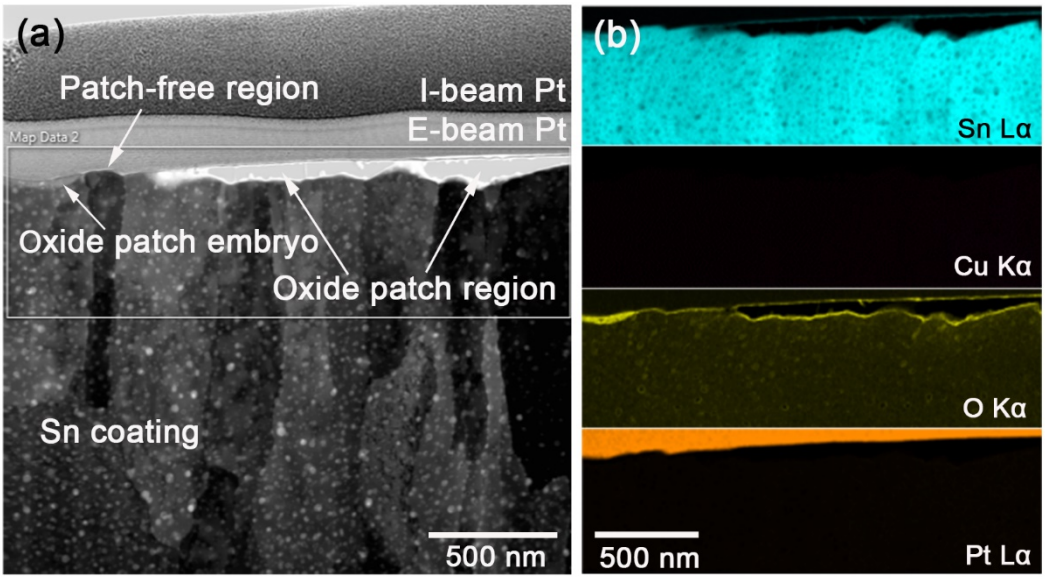

Figure 3 – a) STEM bright field image showing the representative cross-sectional microstructure of the surface region of a 2.5 μm thick pure Sn finish on Cu substrate after isothermal ageing at 155°C in air for 12 hr, and b) its corresponding EDX maps.

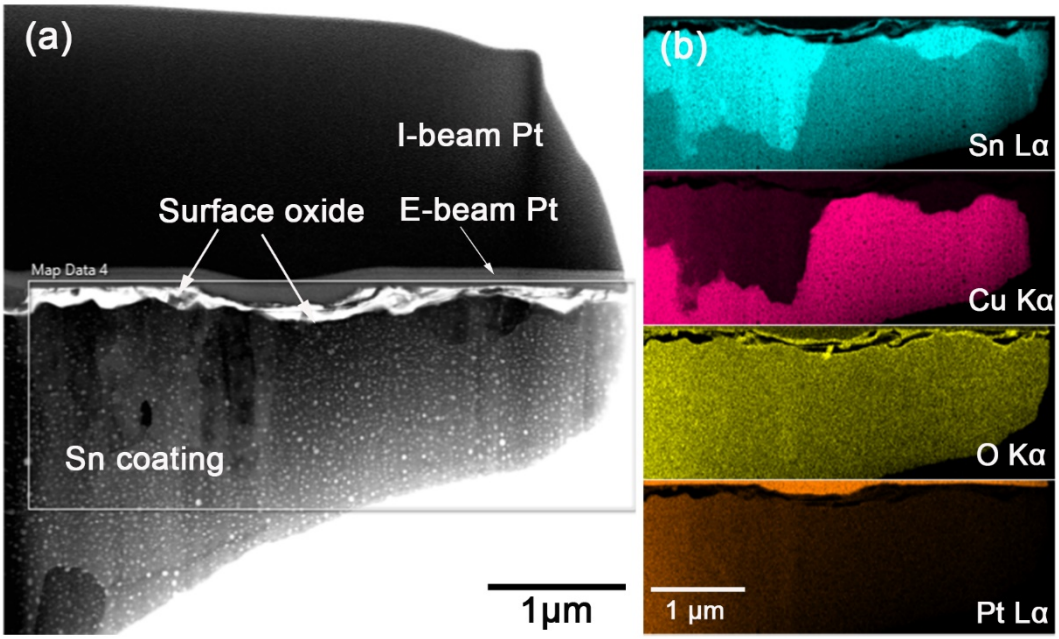

Figure 4 – a) STEM bright field image showing the representative cross-sectional microstructure of the surface region of a 2.5 µm thick pure Sn finish on Cu substrate after isothermal ageing at 155°C in air for 16 hr, and b) its corresponding EDX maps.

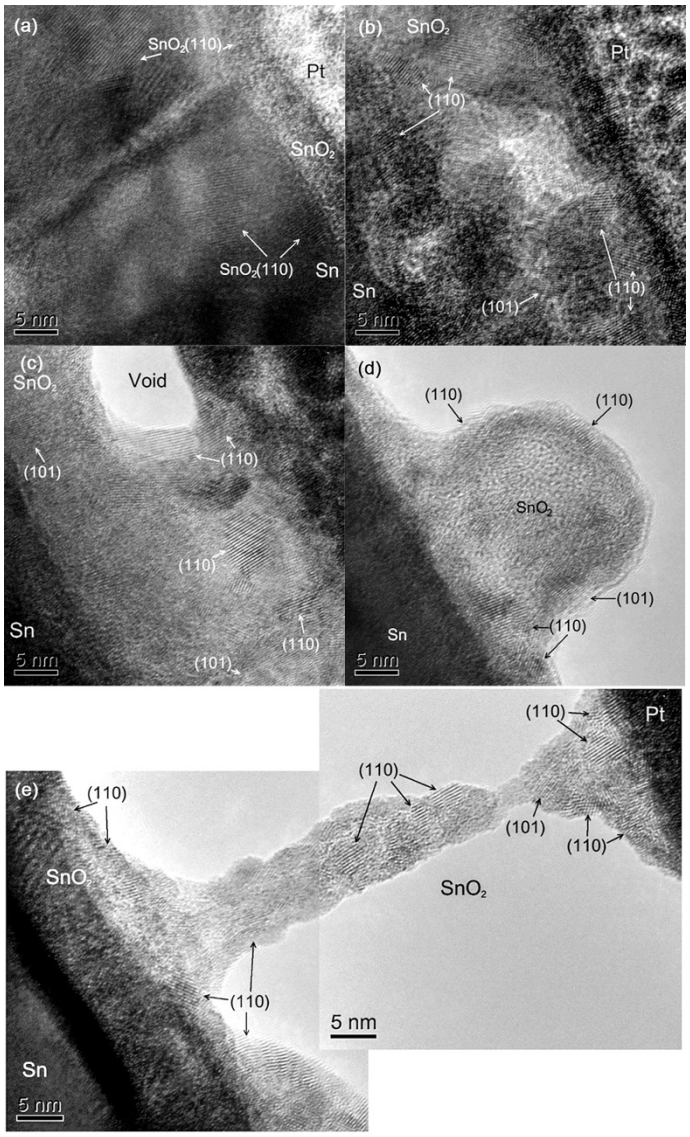

Figure 5 – HRTEM images depicting the representative cross sectional morphology of surface oxides thermally grown on 2.5 μm thick Sn metal films over Cu substrate at 155°C in air after 12 hr: a) in a patch-free region; b) in an embyro patch region; c-d) in a developed patch region and e) oxide platelet in a developed patch region

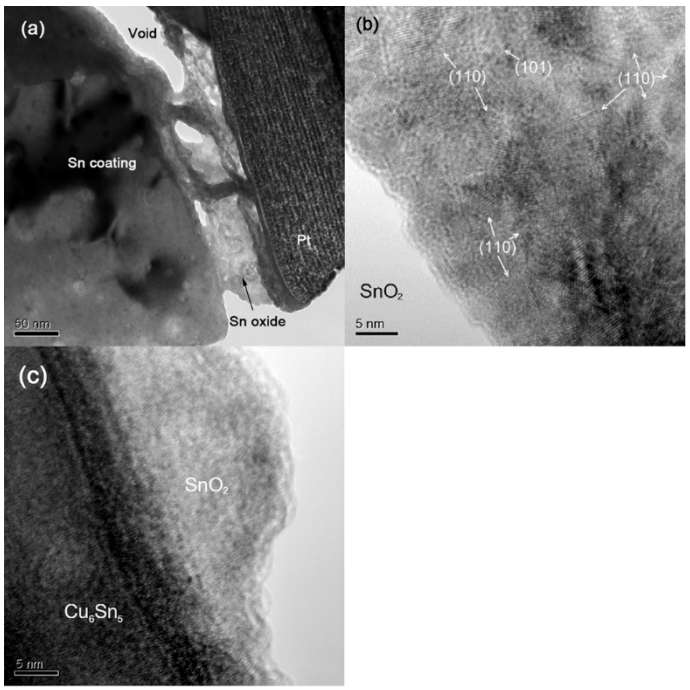

Figure 6 – TEM images depicting the representative cross sectional morphology of surface oxides thermally grown on 2.5 µm thick Sn metal films over Cu substrate at 155°C in air for 16 hr: a) low magnification showing the presence of caviety in the oxide; HRTEM images showing b) representative oxide microstructure and c) oxide microstructure on the exposed IMC surface

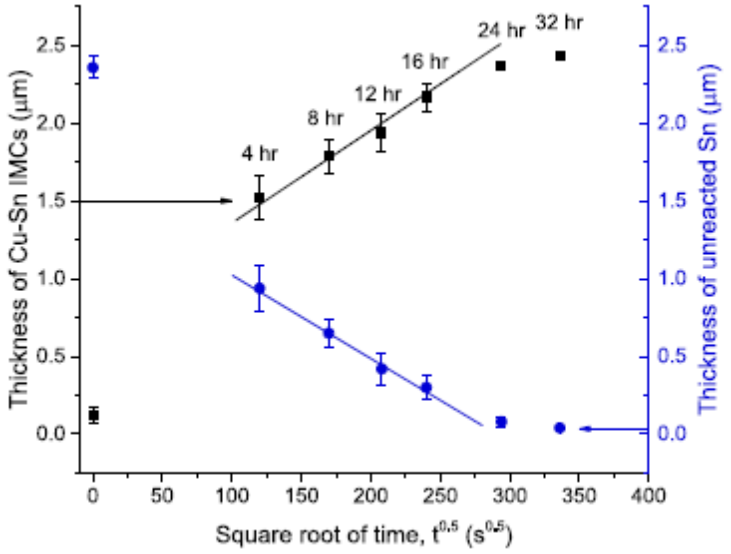

Figure 7 – A plot showing the average thicknesses of interfacial Cu-Sn IMCs and unreacted Sn of 2.5 µm thick pure Sn on Cu samples as a function of the square root of isothermal ageing time at 155°C

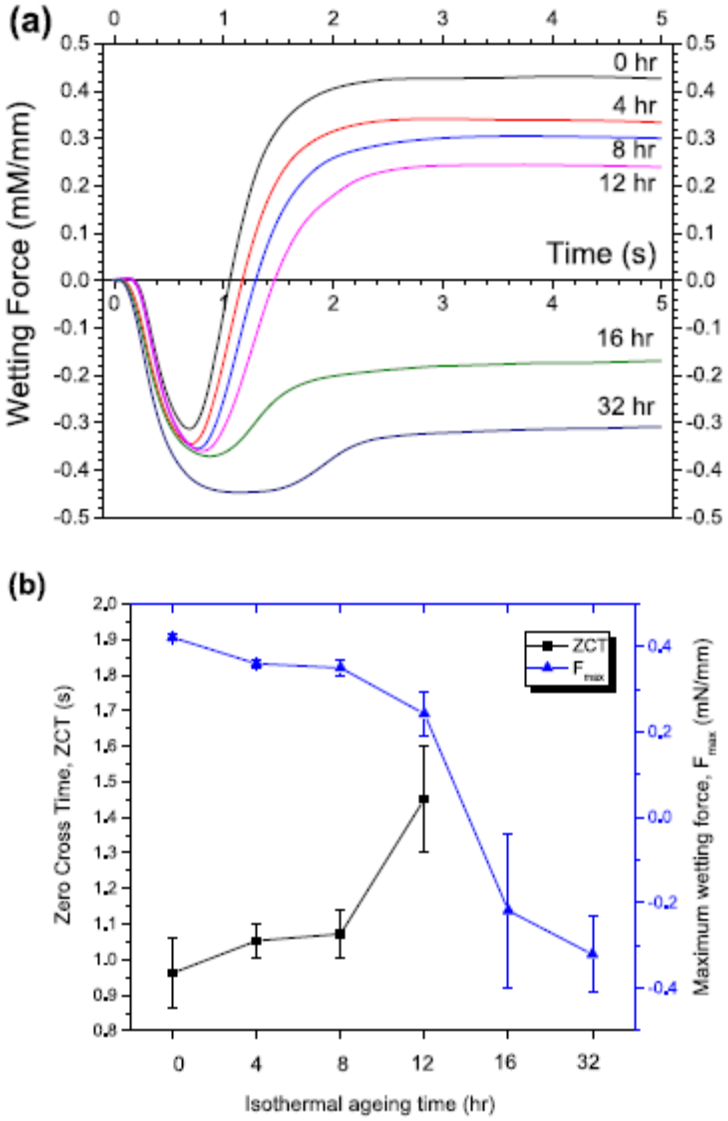

Figure 8 – a) A plot of representative wetting balance force curves as a function of isothermal ageing time and b) a plot showing the effect of thermal ageing time on the zero cross time (ZCT) and maximum wetting force (F_{max}) extracted from the wetting force curves of 2.5 μm thick Sn on Cu samples

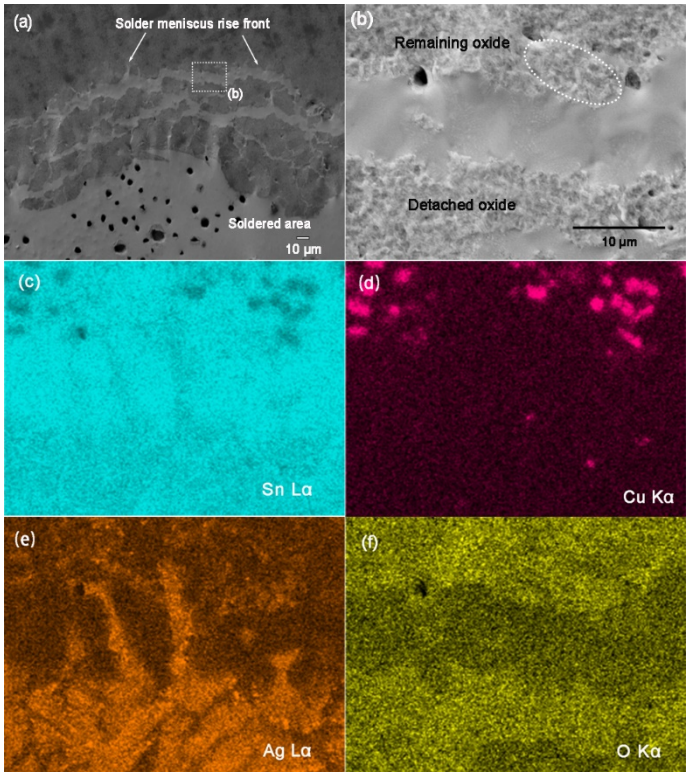

Figure 9 – a-b) SEM images of the representative surface morphology of meniscus rise front of SAC305 solder on a 2.5 µm thick Sn film on Cu sample after 12 hr of thermal ageing at 155°C and wetting balance test and c-f) the corresponding EDX maps of b)

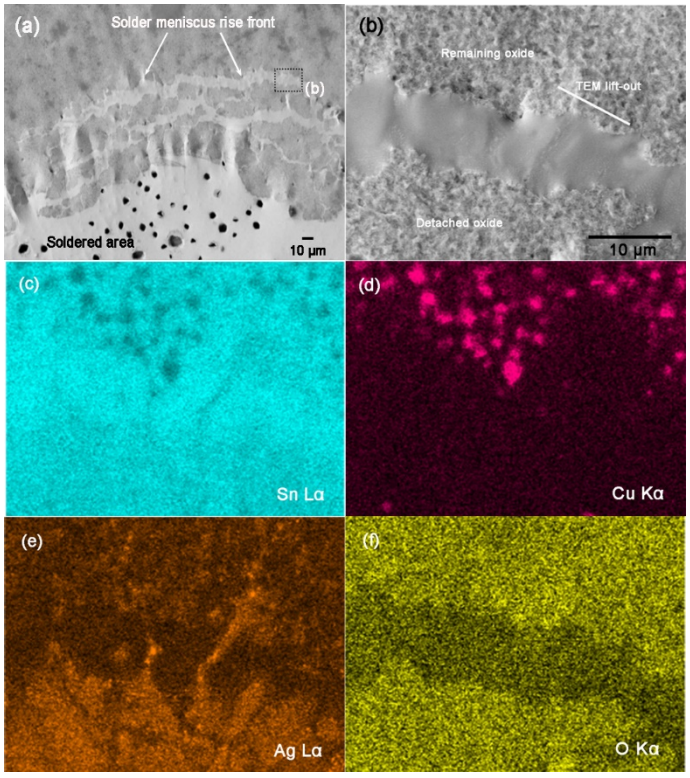

Figure 10 – a-b) SEM images of the representative surface morphology of meniscus rise

front of SAC305 solder on a 2.5 µm thick Sn film on Cu sample after 16 hr of thermal ageing at 155°C and wetting balance test and c-f) the corresponding EDX maps of b)

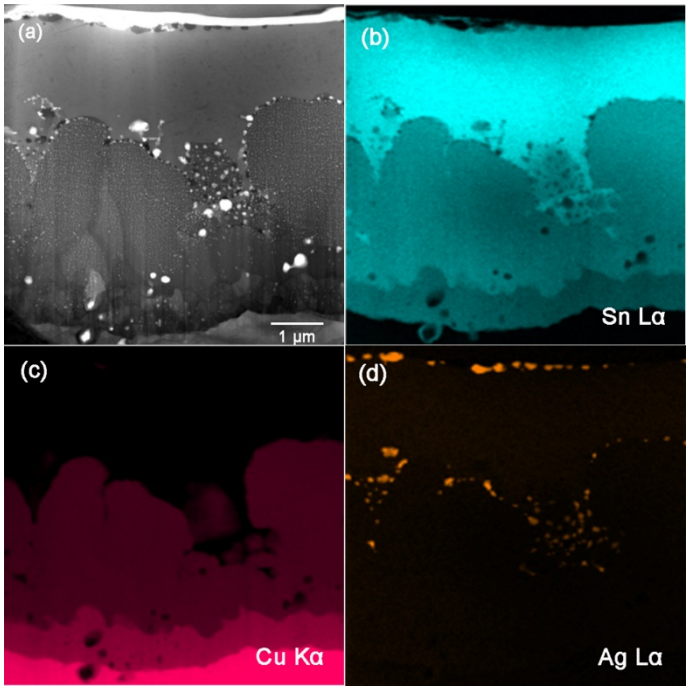

Figure 11 – a) STEM bright field image of the representative cross-section of meniscus rise front of SAC305 solder on a 2.5 µm thick Sn film on Cu sample after 16 hr of thermal ageing at 155°C and wetting balance test and b-d) the corresponding EDX maps.

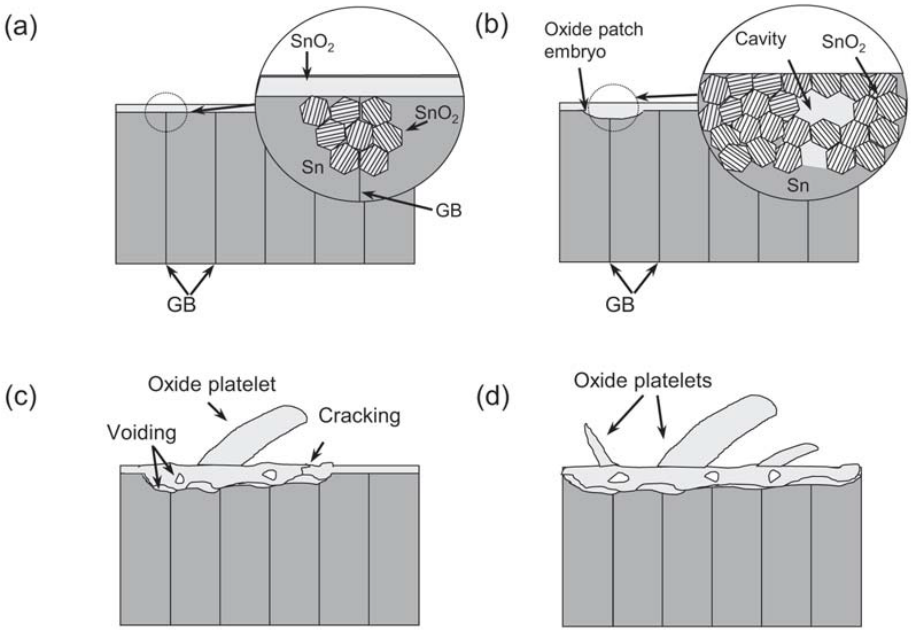

Figure 12 – Cross-sectional schematic diagram showing the evolution of surface oxide of the 2.5 µm thick Sn on Cu sample subject to thermal ageing at 155°C in air

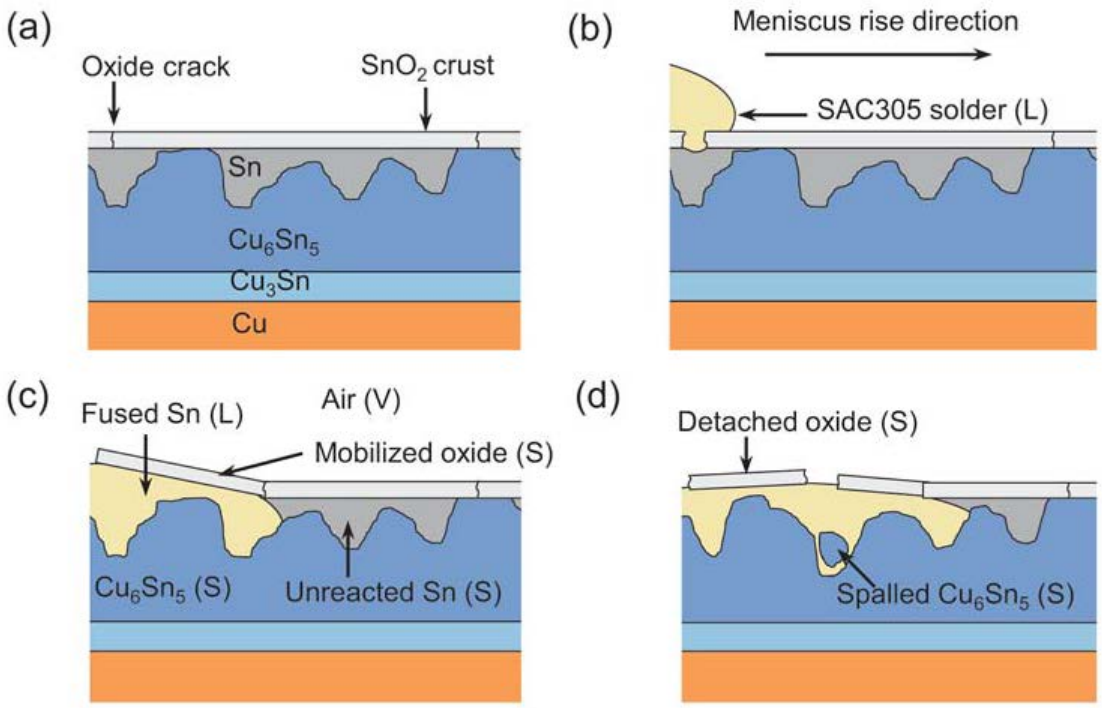

Figure 13 – Cross-sectional schematic diagram showing the evolution of meniscus rise front of the 2.5 μm thick Sn on Cu sample after thermally ageing at 155°C for 16 hr